Radius Determination of Exoplanets and the Typicality of Earth

Haley Bates-Tarasewicz

Abstract

Understanding exoplanets is key to understanding the typicality of our own solar system. The creation and evolution of Earth cannot be understood without first understanding how other planets are created and evolve. Knowing how common earth-like planets are is a start to understanding how representative our own system is as a whole. Exoplanet radii were determined using the transiting exoplanet method to allow comparison of physical traits between extrasolar planets and the planets orbiting our sun. All exoplanets imaged were of comparable size to Jupiter. However, due to the limitations of both the transit method and the observation site, only large exoplanets were able to be

detected. Better equipment must be used before these findings can be understood in context.

Introduction

Exoplanets are planets that orbit star systems other than our own. Exoplanets can be detected in a variety of ways, one of which is via photometric transits. Transits occur when a star system is aligned with Earth such that a planet orbiting will appear to pass in front of, or transit, the host star. In this way, the planet blocks some of the light from the host star, causing a distinctive dip in the light curve[1]. The planets that can be detected with this method are occasionally quite different from Earth[2]. Large planets with close orbits around their host stars known as "Hot Jupiters" are found disproportionately, which makes our own star system seem atypical by comparison[3].

Studying exoplanets can help further understanding of the underlying mechanisms of planet formation. To understand how planets form, it is useful to know how similar planets in other star systems are to our own Earth. By analyzing the light curve produced when an exoplanet transits its host star (Figure. 1) the radius of the planet can be deduced[4].

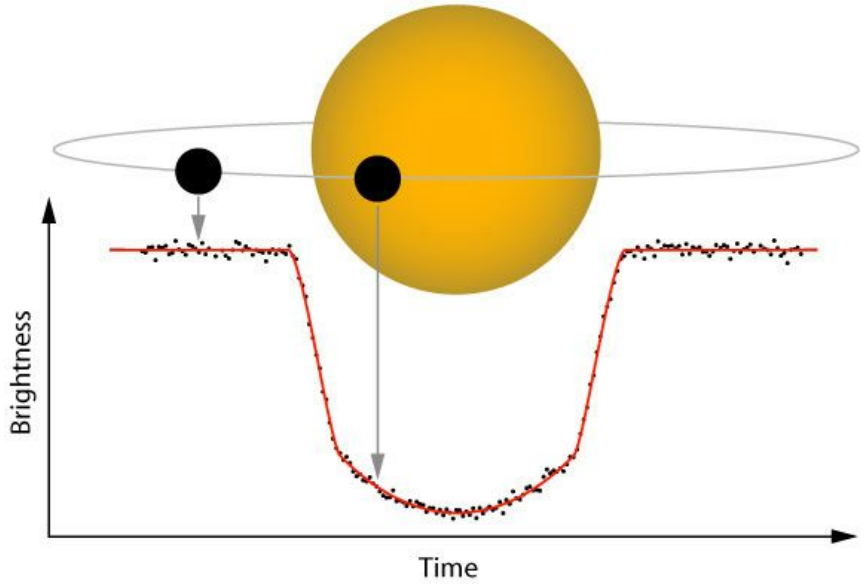

Figure 1: The transit method of detecting and imaging exoplanets

(Introduction to Differential Photometry. (2013, February 18). Retrieved November 1, 2015)

1 Schneider, J. et al. 2011

2 Marcy, G. et al. 2005

3 Udry, Stéphane et al. 2007

4 Weiss, Lauren M. et al. 2014

Determining any physical properties of exoplanet can be used to learn more about the star system as a whole[5]. Knowing more about the physical properties of planets (radius, mass, composition, etc) outside our solar system can help to better understand the planets within it.

Four exoplanets were observed using the transit method during the months of September and October (2015). From the dip in the observed light curve, the radii of the planets were determined and compared to Jupiter to better understand how other planets compare to those within our own system.

Targets

All transit candidates were observed between September and October 2015 at MIT's Wallace Astrophysical Observatory.

Candidates were chosen such that the magnitude of the host star was well within the lower limit detectable with the equipment at Wallace (~18th magnitude)[6]. Transit candidates were also chosen such that the depth of transit is visible with the resolution of the available instrumentation (~ 10 milimags)[7]. Transit candidates were optimized such that the entirety of the transit would be viewable in one night, considering both elevation and duration. To be visible at Wallace Observatory, a target must be above 20° in elevation, and due to travelling restrictions, the full transit must be less than 3h total[8]. Full observational circumstances for each target are located in Table 1 below.

5 Seager, S. et al. 2007

6 Brothers, T., 2015

7 Brothers, T., 2015

8 Brothers, T., 2015

Table 1: Observational Circumstances for Observed Exoplanet Transits at Wallace Astrophysical Observatory in September and October

Date (EDT)	Transit	Apparent Magnitude (R)	Delta Magnitude (milimags)	Elevation (start, mid, end)	Time (EDT) (start, mid, end)	Right Ascension (J2000)	Declination (J2000)
9/14/2015	Tres-3 b	12.1	29.3	37°, 30°, 24°	22:44—23:24—00:04	17 52 07.02	+37 32 46.2
10/5/2015	Tres-1 b	11.2	19.8	53°, 39°, 26°	22:01—23:16—00:31	19 04 09.84	+36 37 57.5
10/16/2015	Kepler-6 b	15.6	10.4	72°, 52°, 34°	20:25—22:23—00:21	19 47 20.94	+48 14 23.8
10/25/2015	Kepler-45 b	15.7	34.2	77°, 71°, 65°	20:53—21:25—21:57	19 31 29.50	+41 03 51.3

(This research has made use of the VizieR catalogue access tool, CDS, Strasbourg, France. The original description of the VizieR service was published in A&AS 143, 23
Source of transit specifications: The USNO-A2.0 Catalogue. (1998). Retrieved November 1, 2015)

All data were to be analyzed via on chip standard stars. Standard stars were chosen such that they were easily in the target star field during observation, and care was taken to ensure they were within 1.5 magnitudes of the target star.

Effort was made to pick comparison stars brighter than the target, so the signal to noise ratio would be limited by the target star rather than the comparison star. In many cases, however, choosing slightly dimmer stars was unavoidable simply due to the stars available on chip.

Three comparison stars for each transit were considered. Table 2 below shows the specifications for each comparison star according to the transit candidate. Complete finder charts for each transit candidate are located in the appendix.

Table 2: Comparison Star Specification for Transit Star Fields (see appendix for finding charts)

Transit	Right Ascension (J2000)	Declination (J2000)	Magnitude (R)
Tres-3 b	17 52 18.57	+37 35 56.22	13.4
	17 52 5.36	+37 30 42.48	13.9
	17 51 42.88	+37 31 13.12	13.0
Tres-1 b	19 04 09.35	+36 39 20.09	12.8
	19 04 07.91	+36 40 11.97	11.2
	19 03 39.34	+36 37 25.94	10.7
Kepler-6 b	19 47 08.6	+48 15 28.58	14.4
	19 47 00.23	+48 17 06.73	12.6
	19 46 55.64	+48 12 25.92	14.0
Kepler-45 b	19 31 31.91	+41 04 54.22	15.1
	19 31 20.60	+41 02 12.04	15.4
	19 31 29.46	+41 01 13.21	14.9

(This research has made use of the VizieR catalogue access tool, CDS, Strasbourg, France. The original description of the VizieR service was published in A&AS 143, 23
Source of specifications: The USNO-A2.0 Catalogue. (1998). Retrieved November 1, 2015)

Methods of Observation

All data were taken at Wallace Astrophysical Observatory. Two telescopes were used to collect data were the Ealing 16” telescope, and 14” Celestron telescope (Pier 3).

Both telescopes used in data collection made use of an SBIG STL-1001E CCD Camera. Full specifications for both telescopes and the camera are located in Tables 3, 4, and 5 below.

Table 3: Specifications for Ealing 16" Telescope[1]

Diameter (inches)	16
Focal Length (mm)	4429.8
Primary Instrument	SBIG STL-1001e
Field of View (arcminutes)	19.07 x 19.07
Plate Scale (arcseconds/pixel)	1.11
Filters	Clear, B, V, R, I, VR

(Brothers, T. (2015, June 18). Retrieved November 1, 2015)

Table 4: Specifications for 14" Celestron C14 Schmidt-Cassegrain Telescope[1]

Diameter (inches)	14
Focal Length (mm)	3910
Primary Instrument	SBIG STL-1001e
Field of View (arcminutes)	20.65 x 20.65
Plate Scale (arcseconds/pixel)	1.21
Filters	Clear, B, V, R, I, VR

(Brothers, T. (2015, June 18). Retrieved November 1, 2015)

Table 5: Instrumental Specifications for SBIG STL-1001E CCD Camera[1]

Min / Max Exposure Times (sec)	0.01 / 3600
Max Counts Unbinned	~64000
Gain (electrons)	2.0
Pixel array	1024 x 1024 active element
Pixel dimensions (square microns)	24
Working Temperature Range (deg C)	-15 to -25

(Brothers, T.(2015, June 18). Retrieved November 1, 2015.)

Data

Four nights of data were taken over the months of September and October 2015. Each night, the the telescopes were set up in accordance with Wallace Observatory's instructions and guidelines and focused. The telescopes were then slewed to the correct right ascension and declination of the target transit candidate, star hopping to the correct target.

Each night before any data was taken, 10 0s exposure bias frames were taken as a diagnostic tool as well as for use in later data reduction.

Exposure times for science frames were determined by a combination of TA input and adjustment so the counts from the target star fell on the linear range of the CCD. The R filter was used for all data as all transit candidates and comparison stars were brightest in the R band. The use of the R filter was not ideal, and in future studies, an alternative method would be to use a clear filter so all light from the star is recorded, maximizing the possible signal. After the exposure time and filter was set, data were taken until time constraints dictated we leave Wallace (usually 3.5hours).

Once science frames were taken, 10 closed-shutter dark frames with exposure times matching that of the science frames were taken for later calibration.

A full breakdown of all data and calibration images taken in September and October is located in Table 6 below.

Table 6: Data Taken at Wallace Astrophysical Observatory in September and October 2015

Transit	Date (2015) (EDT)	Frame	Exposure Time (seconds)	Filter	Data Amount (Images)	Weather	Telescope
Tres-3 b	Sep. 14	Bias	0	n/a	10	Clear	Ealing 16in
		Dark	20	n/a	10		
		Light	20	R	382		
Tres-1 b	Oct. 5	Bias	0	n/a	10	Clear	Ealing 16in
		Dark	30	n/a	10		
		Light	30	R	354		
Kepler-6 b	Oct. 16	Bias	0	n/a	10	Clear	14in Celestron
		Dark	20	n/a	10		
		Light	20	R	716		
Kepler-45 b	Oct. 25	Bias	0	n/a	10	Cloudy	14in Celestron
		Dark	75	n/a	10		
		Light	75	R	173		

Data Reduction and Preliminary Analysis

All reduction of data was done in AstroImageJ.

The calibration frames (bias, dark, flat) were first averaged together to create master bias/dark/flat frames. Bias and dark frames were taken each night of data collection, however because of time constraints, sky flats were not able to be collected, so dark-subtracted library flats were used instead.

First the master bias was subtracted from all frames to remove the counts produced by the camera reading out an image. Then the master dark is subtracted from the science

frames to remove the counts produced by the camera during an exposure. Then, the science images are divided by the reduced flats to remove any imperfections with the telescope or imaging equipment. Figure 2 below illustrates this process.

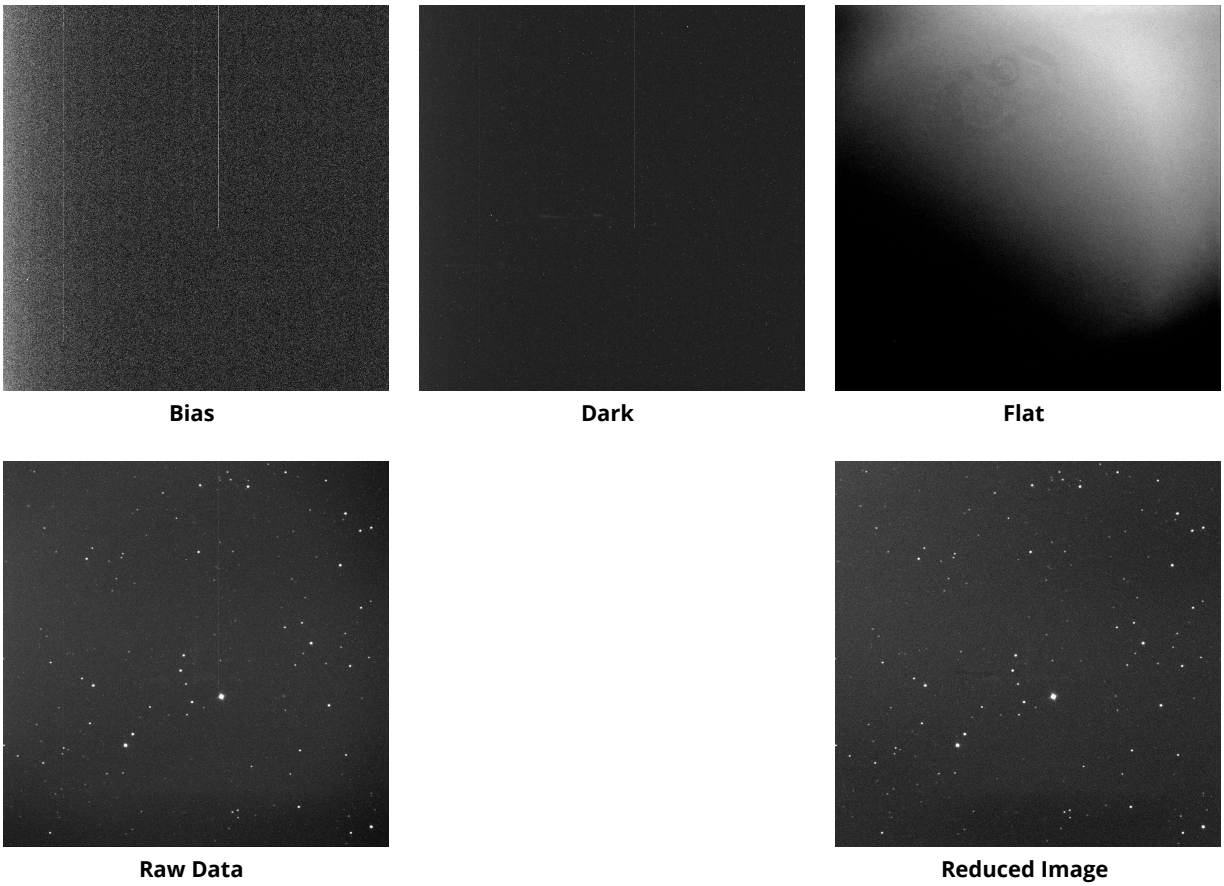

Figure 2: Calibration images and reduction process using dark/bias subtraction and flat division.

After images were reduced, they were analyzed using multi-aperture photometry in AstroImageJ. AstroImageJ uses circular apertures with a concentric background annulus positioned such that little to no target starlight bleeds into it. Aperture and annulus sizes were determined by plotting the seeing profile of the target star and adjusting AstroImageJ's recommended values such that the source aperture contained all relevant source signal, and the background contained no source from stars. An example can be seen in Figure 3 below. Other seeing profiles and apertures/annuli for other nights can be seen in the Appendix.

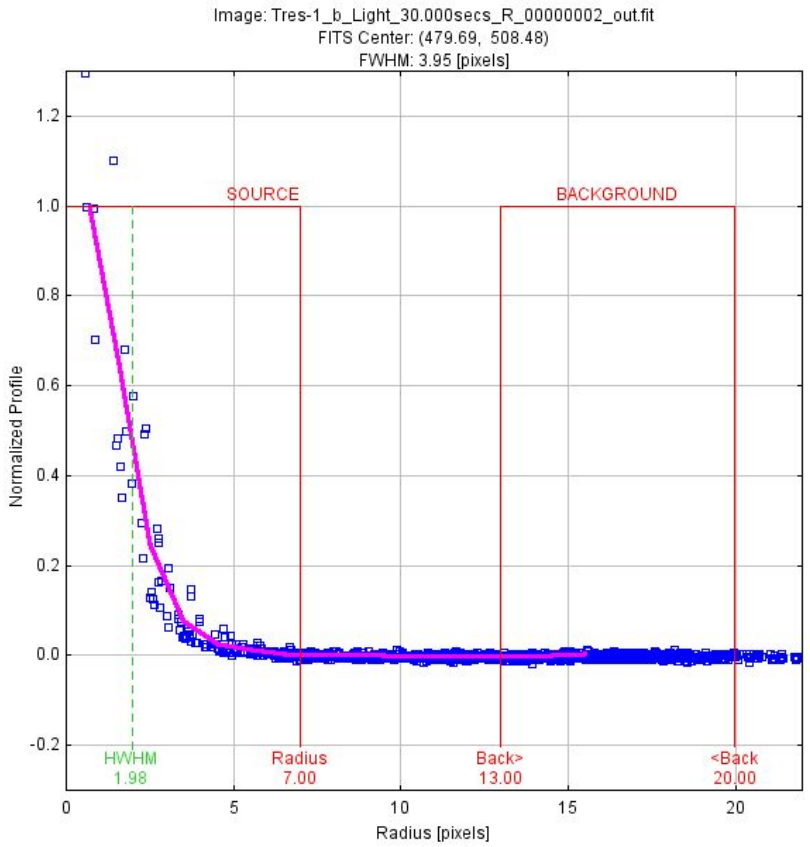

Figure 3: Seeing profile and aperture/annulus radii for Tres-1 b (see other seeing profiles etc. in Appendix)

To ensure that the comparison stars weren't influencing the data, all comparison stars were tested for quality before analysis began. Stars were checked for uniformity by first calculating the relative flux. This was done by dividing the flux from the one star by the combined flux of all other comparison stars. Relative Flux vs Time was then plotted for to verify that each star was a good constant. All comparison stars were verified in this way. An example of one of these comparison star tests can be seen in Figure 4 below. For comparison star verifications of other nights of data, see the Appendix.

Figure 4: Comparison star quality test for Tres-1 b to determine flux uniformity (see other comparison star quality tests in Appendix)

Once all comparison stars were verified as constant over the course of the night, they were used to analyze the target transit candidate. Multi-aperture photometry was again done in AstroImageJ. The relative flux of the transit candidate to the average of the target stars was recorded. Figure 5 below shows the aperture and target locations for one night. Other nights can be seen in the Appendix.

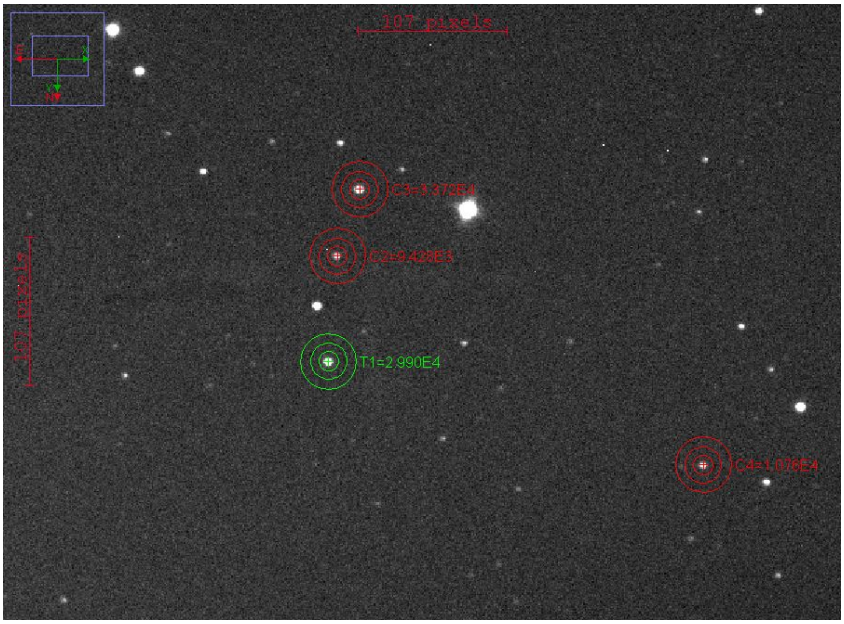

Figure 5: Comparison stars and multi-aperture photometry processing for Tres-1 b (see other aperture placement and comparison stars in Appendix)

Table 7 details the aperture and annulus radii for all datasets, as calculated by the method discussed in Figure 3 above.

Table 7: Apertures and background annuli for multi-aperture photometry

Transit	Radius of Object Aperture (px)	Inner Radius of Background Annulus (px)	Outer Radius of Background Annulus (px)
Tres-3 b	6	11	17
Tres-1 b	7	13	20
Kepler-6 b	6	11	17
Kepler-45 b	5	9	14

Once the relative flux of the target transit candidate to the comparison stars was calculated, it was plotted and analyzed in MATLAB. All four nights were plotted in this manner. Out of all four nights, only the plot below (Figure 6) of data taken of Tres-1 b on 10/05/2015 showed a transit dip.

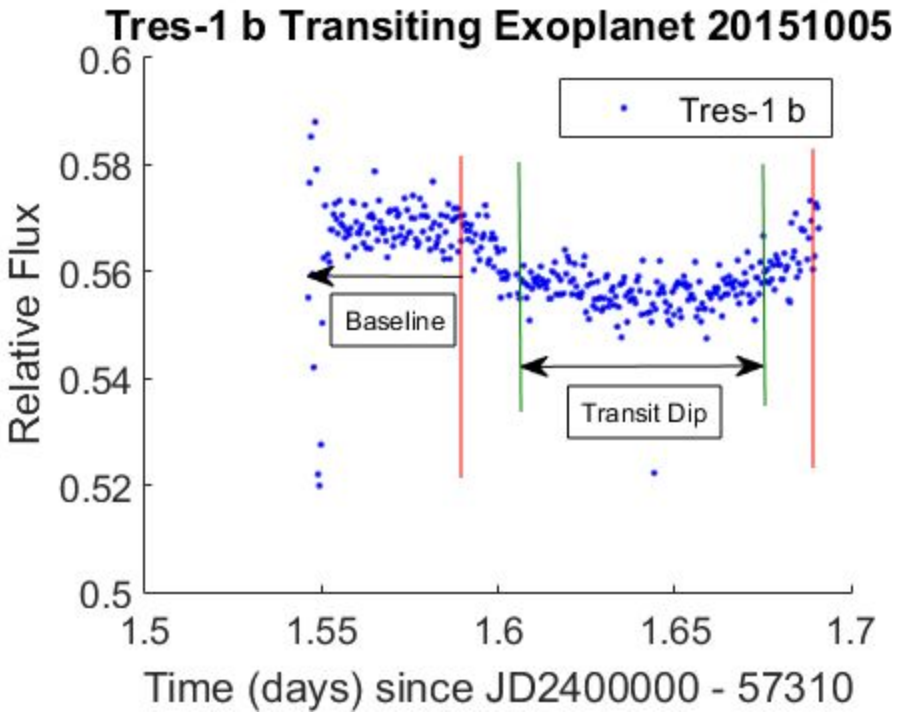

Figure 6: Relative Flux vs Time of transiting exoplanet Tres-1 b on October 5th 2015 (see other relative flux plots in Appendix)

Figure 7 shows the relative flux vs time of the data taken of Tres-3 b on 9/14/2015. There was unfamiliarity with the software used to plan transit observations, and due to an unfortunate mistake, the observation took place on the wrong night. For these data, no transit dip was expected. The sudden spike and break in the data are due to cloud interference.

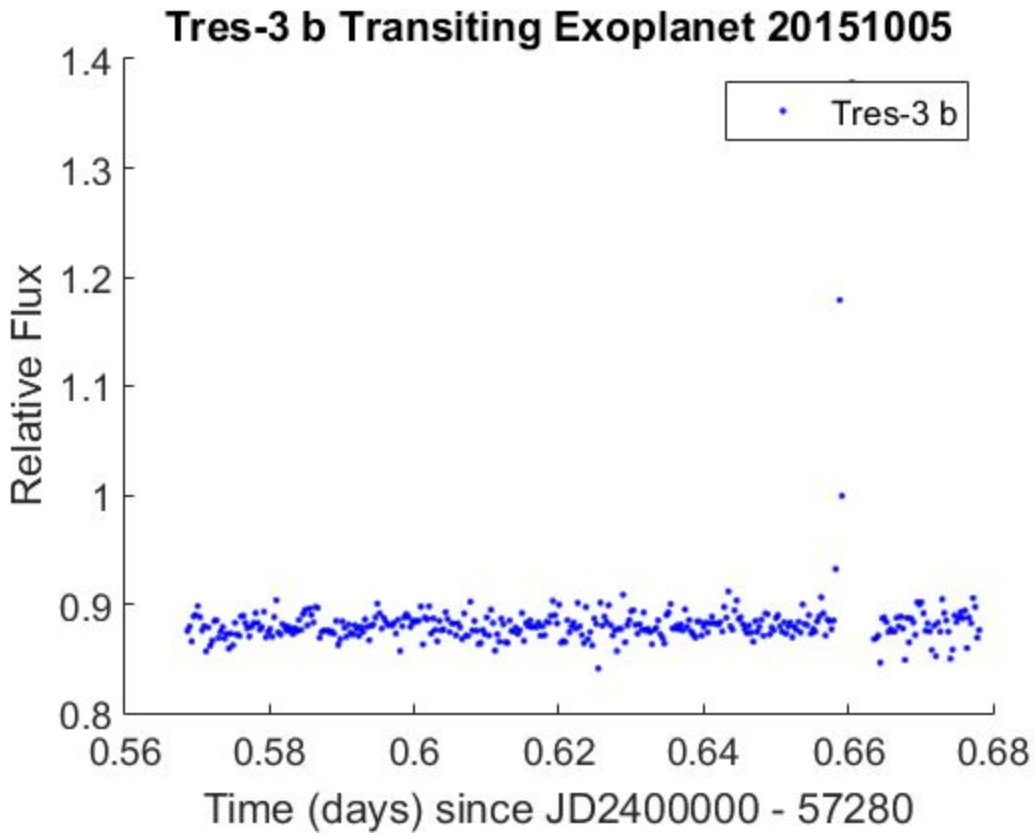

Figure 7: Relative Flux vs Time of transiting exoplanet Tres-3 b on September 14th 2015

Figure 8 below shows a similar plot of relative flux vs time of data taken of Kepler-6 b on 10/16/2015. This plot does not show a dip; However, the predicted depth of transit was only 10.4 milimags, which is right at the very lower limit of the capabilities of Wallace Observatory. It is not surprising that a transit dip was not observed. Problems with dew and clouds caused some scattering in the beginning and middle of the plot.

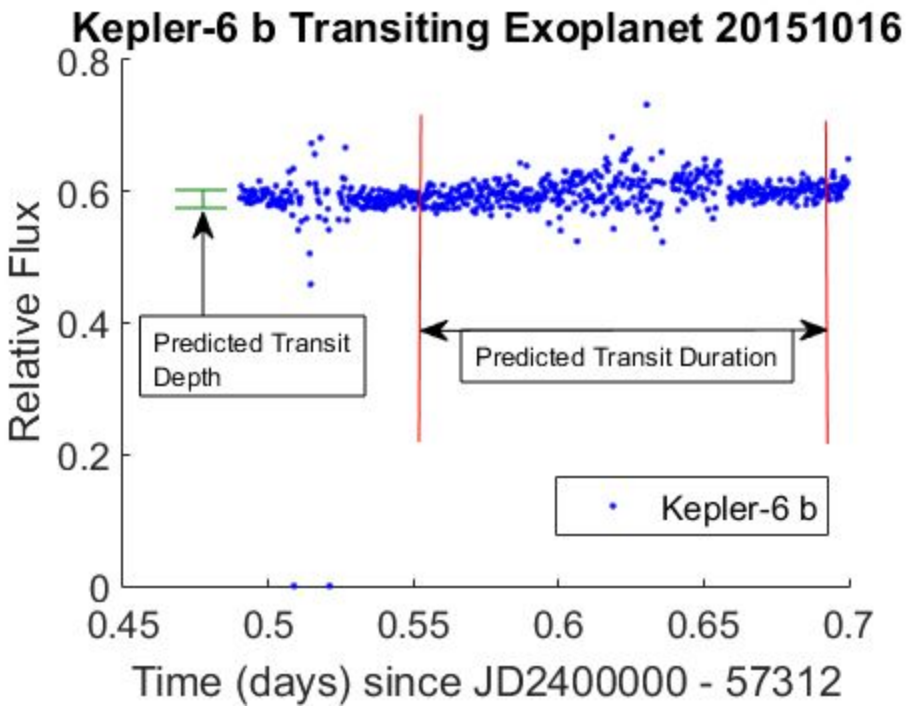

Figure 8: Relative Flux vs Time of transiting exoplanet Kepler-6 b on October 16th 2015

Figure 9 shows the relative flux of Kepler-45 b, taken on 10/25/2015. The night ended up being much cloudier than expected, so most of the data were taken under nearly full cloud cover. After rejecting frames where no stars were visible and only analyzing ones where the target was resolved at all, there wasn't enough data to say that a transit did or didn't occur.

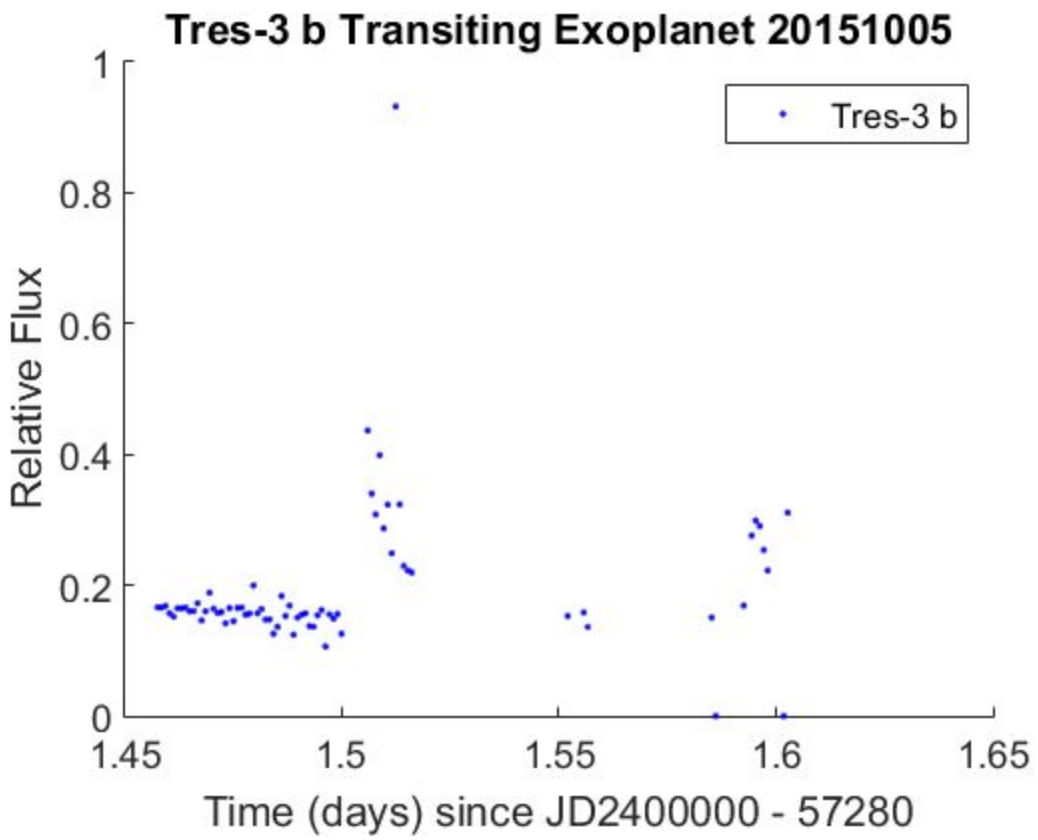

Figure 9: Relative Flux vs Time of transiting exoplanet Kepler-45 b b on October 25th 2015

Because of the challenges with software that resulted in the 9/14/2015 data being unusable, and because of poor weather conditions on 10/25/2015, only the data taken on 10/05/2015 and 10/16/2015 were considered for further analysis.

Results and Analysis

While using the transit method, planetary/stellar radii are related to the transit dip by $\frac{\Delta f}{f} = (\frac{r}{R})^2$ where f is the flux, r is the radius of the exoplanet, and R is the stellar radius [9].

Table 8 shows the published stellar radii in terms of the sun's radius for each analyzable night.

9 Schneider, J. et al., 2011

Table 8: Transiting exoplanet host star physical properties

Transit	Published Stellar Radius (R_{sun})
Kepler-6 b	1.39 ± 0.02
Tres-1 b	0.87 ± 0.02

(This research has made use of the Exoplanet Orbit Database and the Exoplanet Data Explorer at exoplanets.org. Source of stellar radii: (Han, E. et al., 2014))

Analysis for the transit recorded on 10/05/2015 of Tres-1 b began by calculating the mean of both the baseline non-transiting star flux and of the dip base, assuming every data point had the same uncertainty. The Student's t-test was used to ensure the dip was a statistically significant feature and not just a fluke of the data. The certainty that the dip illustrated in Figure 6 is a statistically separate from the baseline was 92%.

The standard deviation for each set was then determined using MATLAB. This and the two means calculated earlier were used to determine the transit depth or the change in flux. The transit depth for the data taken of Tres-1 b on 10/05/2015 was determined to be 0.0059 ± 0.0042.

Taking this number and dividing it by the stellar baseline flux (calculated to be 0.5669) gives a dimensionless number that represents the ratio of the planetary radius to the stellar radius. Using the published stellar radius for the host star of Tres-1 b (Table 8) the exoplanet's radius in terms of Jupiter's radius was calculated to be 1.015 ± 0.035 $R_{Jupiter}$. Comparing this to the published value of 1.067 ± 0.022 $R_{Jupiter}$ using the Student's t test, the difference is not found to be statistically significant.

For the case of the data taken on 10/16/2015 of Kepler-6 b, no transit dip was recorded, so instead the largest possible transit dip given the data was calculated. Analysis began by calculating the weighted mean of the entire dataset at 0.596 using MATLAB. From this, the standard deviation of the entire set was calculated to be 0.039, also using MATLAB.

The largest transit depth that could have taken place is 0.039, which represents the ratio of the planetary radius to the stellar radius squared.

Again using $\frac{\Delta f}{f} = (\frac{r}{R})^2$ and the published stellar radius of the host star of Kepler-6 b (Table 8), the radius of the planet was determined to be a maximum of 3.539 $R_{Jupiter}$. Comparing this to the published value 1.323 ± 0.026, the difference is statistically significant. However, this is unsurprising as the calculated value wasn't expected to match with

previous publications, as the largest possible planetary radius was calculated, not the actual planetary radius.

No data points were rejected for either night of data.

Table 9 shows all of the values calculated in the analysis of both nights of data.

Table 9: Calculated values for the determination of exoplanet radii

Transit	Weighted Mean (baseline, transit dip)	Standard Deviation (baseline, transit dip)	Transit Depth	Calculated Radius ($R_{Jupiter}$)
Tres-1 b	0.5669, 0.5610	0.0086, 0.0079	0.0059 ± 0.0042	1.015 ± 0.035
Kepler-6 b	0.596, n/a	0.039, n/a	0.039 (upper bound)	3.539 (upper bound)

Conclusions

The research done in September and October 2015 at Wallace Astrophysical Observatory on transiting exoplanets leads to several different tentative conclusions to the question of the typicality of our own star system.

It could be that our solar system is very atypical in that it contains very small planets far away from the host star. The two exoplanets analyzed by this research both have large radii comparable to that of Jupiter, and orbit quickly around their host star in a manner very unlike our own system. This could be indicative of a galaxy full of large planets, where small ones are rare or less common.

Far more likely, the limitations of the transit method and the equipment used lead to the detection of only large planets. The transit method as well as the limitations of Wallace Observatory required the transit selected have large transit dips with fast periods. In many cases, planets are too small to block a detectable amount of a host star's light, or orbit too slowly for practical observations to occur at Wallace Astrophysical Observatory. To better understand our own star system, better equipment must be used in order to eliminate the bias towards "Hot Jupiter" planets.

References

Brothers, T. (2015, June 18). Retrieved November 1, 2015.

Han, E., Wang, S., Wright, J., Feng, K., Zhao, M., Fakhouri, O., . . . Hancock, C. (2014). Exoplanet Orbit Database. II. Updates to Exoplanets.org. 126(943), 827-837. Retrieved November 1, 2015, from http://adsabs.harvard.edu

Marcy, G.; Butler, R. P.; Fischer, D.; Vogt, S.; Wright, J. T.; Tinney, C. G.; Jones, H.R. A., 2005. Observed Properties of Exoplanets: Masses, Orbits, and Metallicities. Progress of Theoretical Physics Supplement, No. 158, pp. 24-42

Seager, S.; Kuchner, M.; Heir-Majumder, C. A.; Militzer, B., 2007. Mass-Radius Relationships for Solid Exoplanets. The Astrophysical Journal, Volume 669, Issue 2, pp. 1279-1297

Schneider, J.; Dedieu, C,; Le Sidnaner, P.; Savalle, R.; Zolotukhin, I., 2011. Defining and cataloging exoplanets: the exoplanet.eu database. Astronomy & Astrophysics, Volume 532, id.A79, 11pp

The USNO-A2.0 Catalogue. (1998). Retrieved November 1, 2015)

Udry, Stephane; Santos, Nuno C. 2007. Statistical Properties of Exoplanets. Annual Review of Astronomy & Astrophysics, vol. 45, Issue 1, pp.397-439.

Weiss, Lauren M.; Marcy, Geoffrey W., 2014. The Mass-Radius Relation for 65 Exoplanets Smaller than 4 Earth Radii. The Astrophysical Journal Letters, Volume 783, Issue 1, article id. L6, 7 pp. (2014).

Appendix

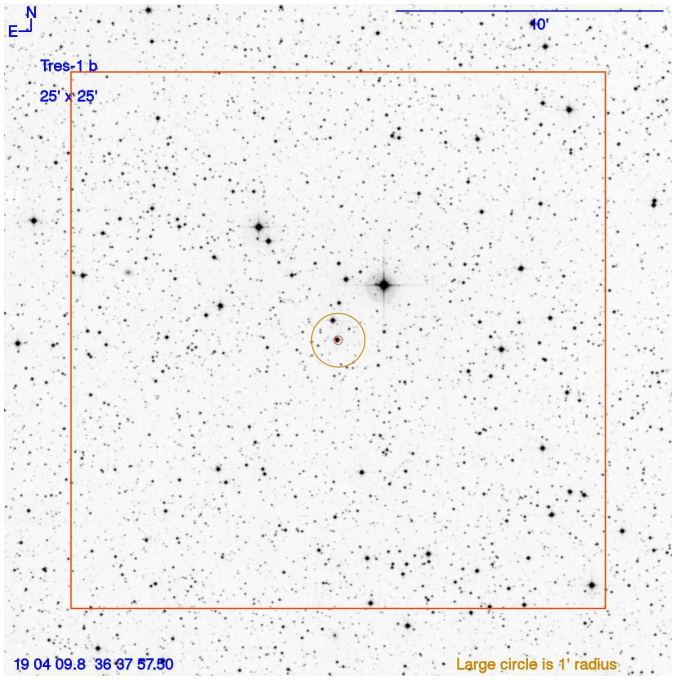

Appendix 1: Tres-1 b finding chart. Target circled in center.

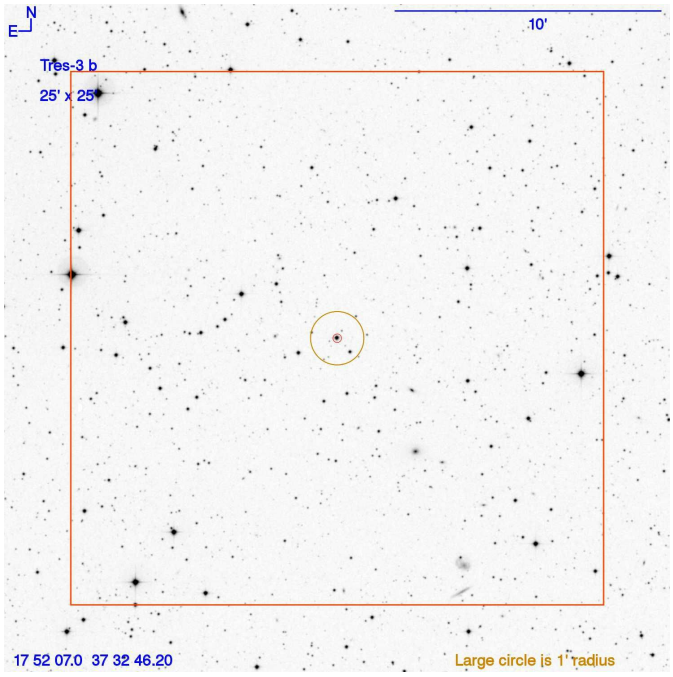

Appendix 2: Tres-3 b finding chart. Target circled in center.

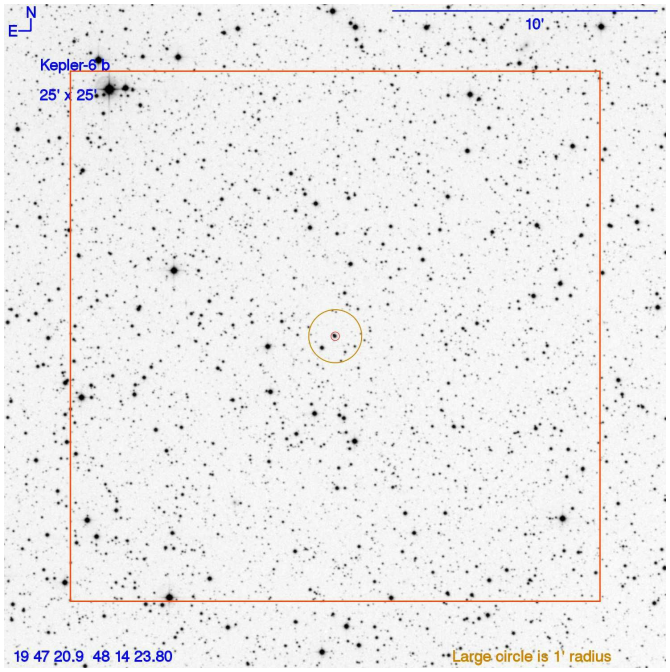

Appendix 3: Kepler-6 b finding chart. Target circled in center.

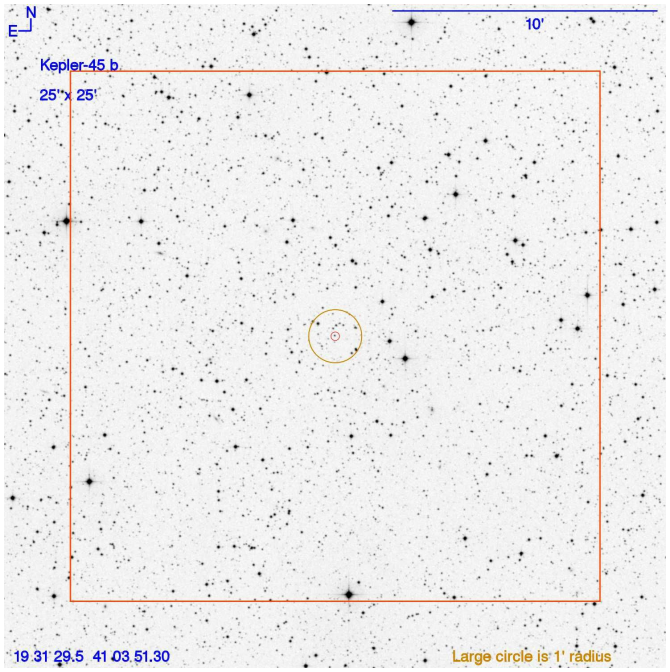

Appendix 4: Kepler-45 b finding chart. Target circled in center.

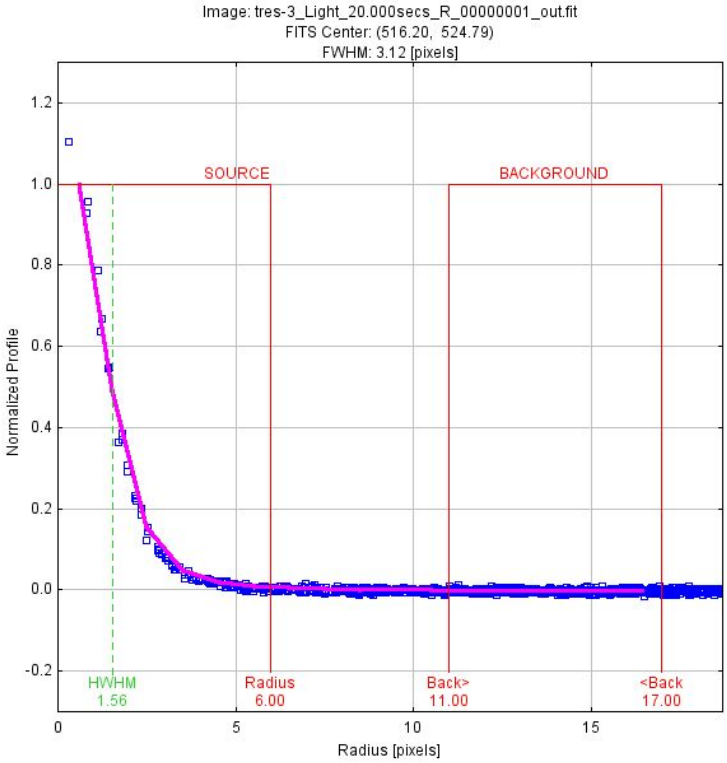

Appendix 5: Seeing profile and aperture/annulus radii for Tres-3 b

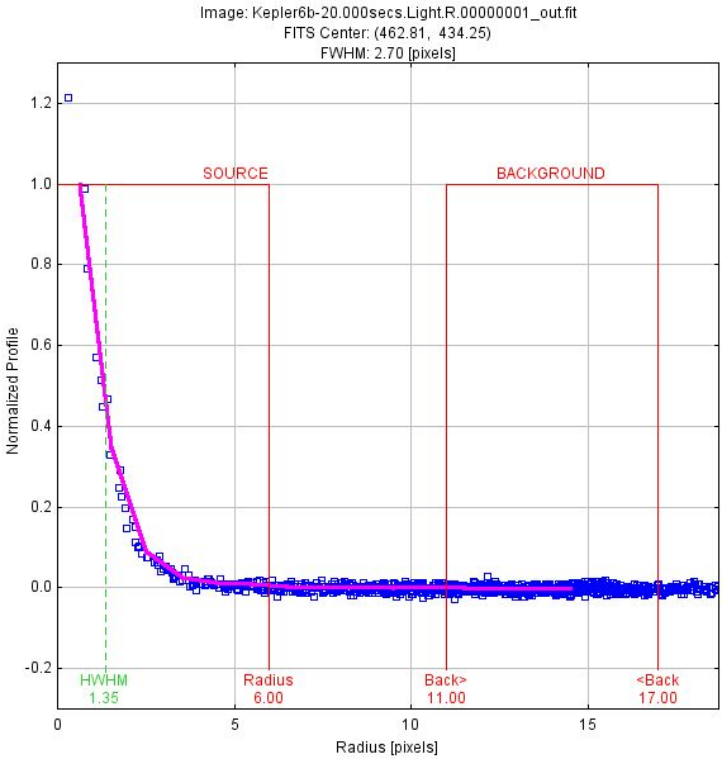

Figure 6: Seeing profile and aperture/annulus radii for Kepler-6 b

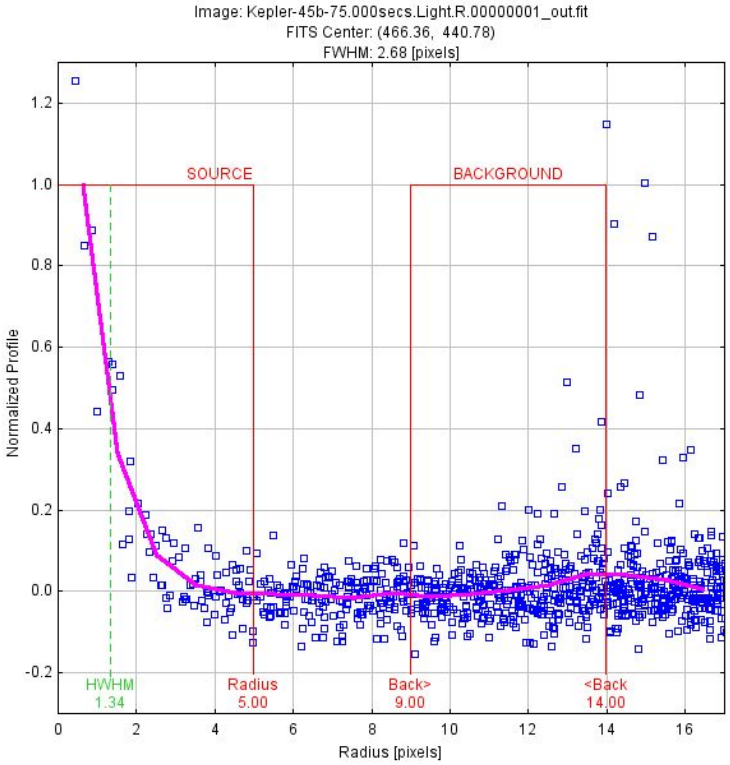

Appendix 7: Seeing profile and aperture/annulus radii for Kepler-45 b

Appendix 8: Comparison star quality test for Tres-3 b to determine flux uniformity

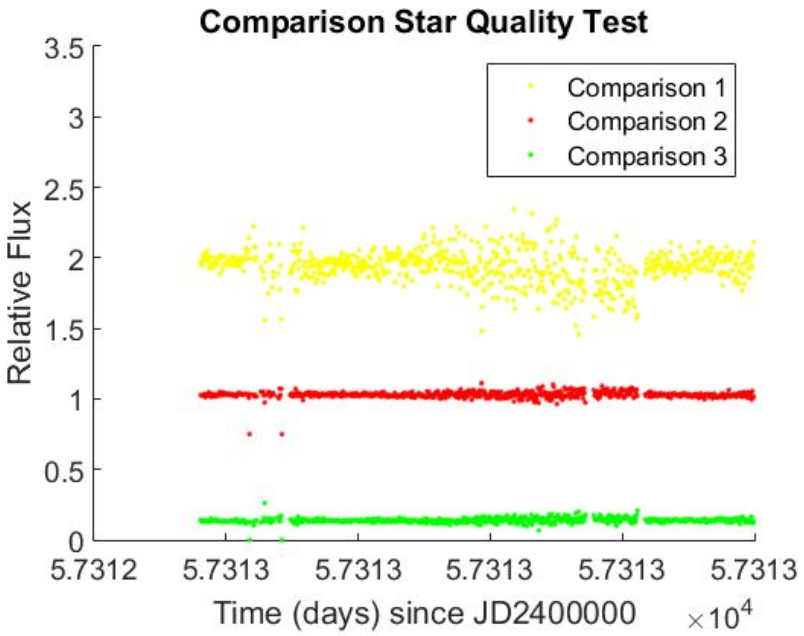

Appendix 9: Comparison star quality test for Kepler-6 b to determine flux uniformity

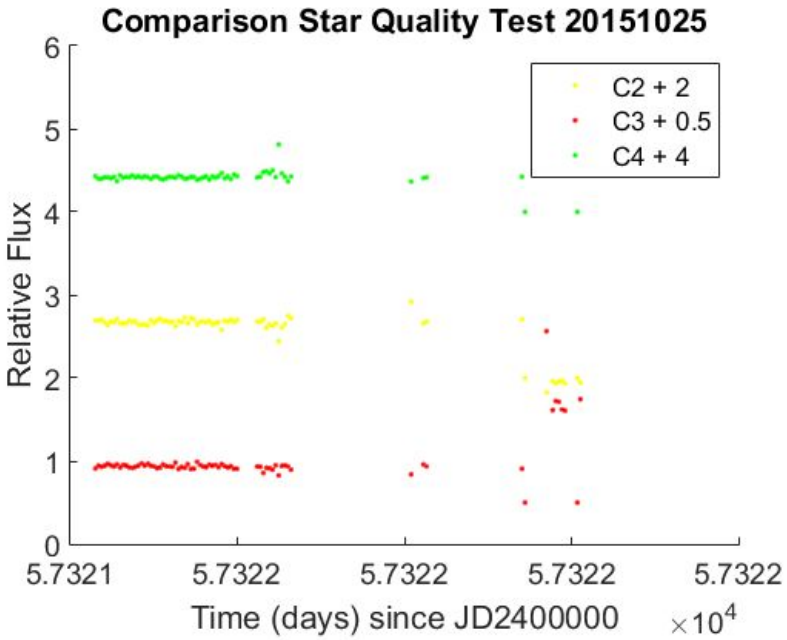

Appendix 10: Comparison star quality test for Kepler-45 b to determine flux uniformity

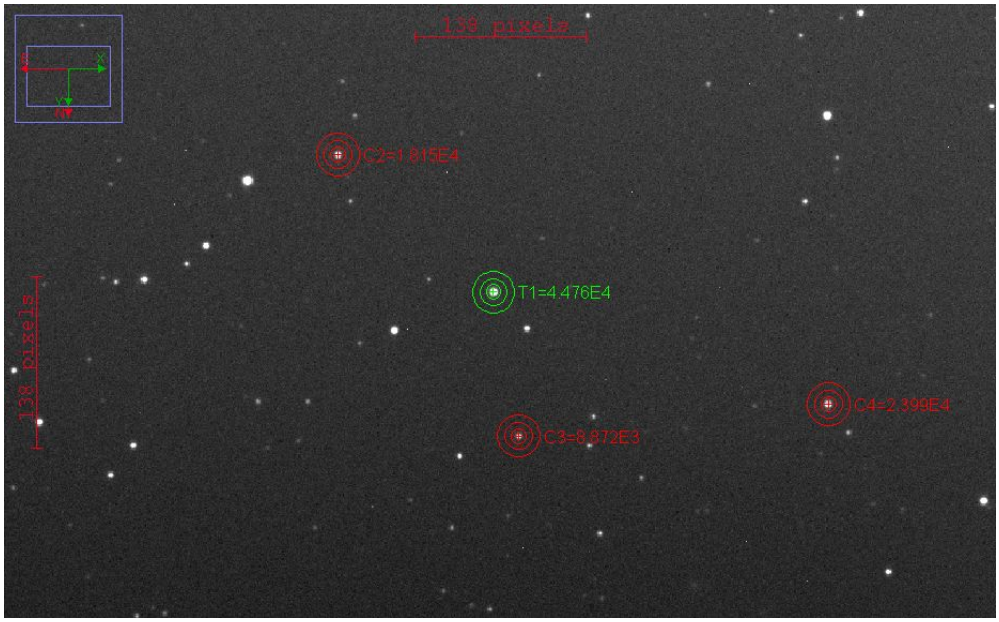

Appendix 11: Comparison stars and multi-aperture photometry processing for Tres-3 b

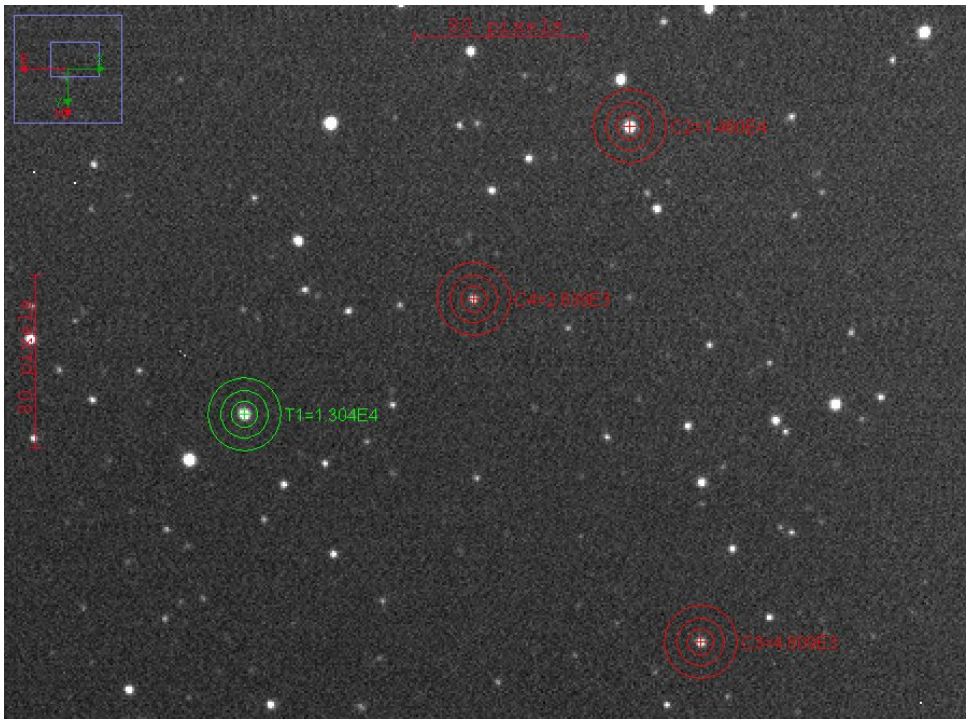

Appendix 12: Comparison stars and multi-aperture photometry processing for Kepler-6 b

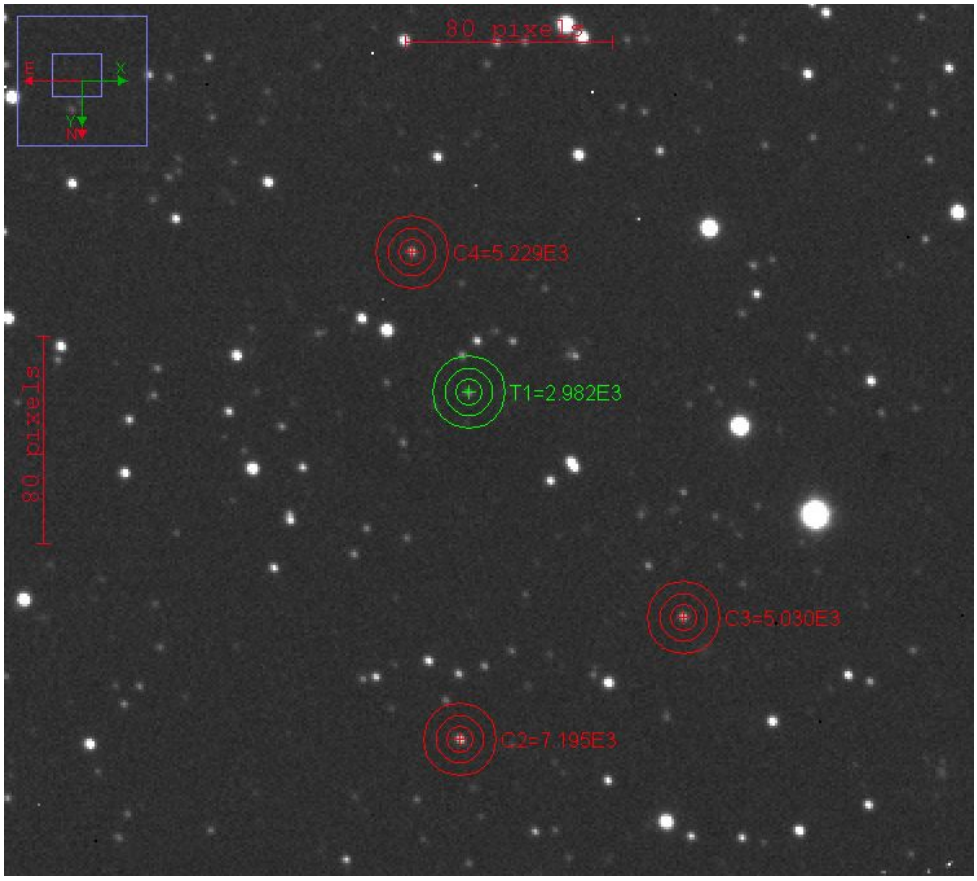

Appendix 13: Comparison stars and multi-aperture photometry processing for Kepler-45 b